

## Structural stability of $\text{Fe}_5\text{Si}_3$ and $\text{Ni}_2\text{Si}$ studied by high-pressure x-ray diffraction and *ab initio* total-energy calculations

D. Errandonea,<sup>1,\*†</sup> D. Santamaría-Perez,<sup>2,3</sup> A. Vegas,<sup>3</sup> J. Nuss,<sup>4</sup> M. Jansen,<sup>4</sup> P. Rodríguez-Hernandez,<sup>5,†</sup> and A. Muñoz<sup>5,†</sup>

<sup>1</sup>*Departamento de Física Aplicada-ICMUV, Universitat de València, Edificio de Investigación, C/Dr. Moliner 50, 46100 Burjassot, Valencia, Spain*

<sup>2</sup>*Max Planck Institute für Chemie, Postfach 3060, D-55020 Mainz, Germany*

<sup>3</sup>*Instituto de Química-Física Rocasolano, CSIC, C/Serrano 119, 28006 Madrid, Spain*

<sup>4</sup>*Max-Planck Institut für Festkörperforschung, Heisenbergstrasse 1, 70569 Stuttgart, Germany*

<sup>5</sup>*Departamento de Física Fundamental II, Universidad de La Laguna, 38207 La Laguna, Tenerife, Spain*

(Received 10 January 2008; revised manuscript received 15 February 2008; published 11 March 2008)

We performed high-pressure angle dispersive x-ray diffraction measurements on  $\text{Fe}_5\text{Si}_3$  and  $\text{Ni}_2\text{Si}$  up to 75 GPa. Both materials were synthesized in bulk quantities via a solid-state reaction. In the pressure range covered by the experiments, no evidence of the occurrence of phase transitions was observed. On top of that,  $\text{Fe}_5\text{Si}_3$  was found to compress isotropically, whereas an anisotropic compression was observed in  $\text{Ni}_2\text{Si}$ . The linear incompressibility of  $\text{Ni}_2\text{Si}$  along the  $c$  axis is similar in magnitude to the linear incompressibility of diamond. This fact is related to the higher valence-electron charge density of  $\text{Ni}_2\text{Si}$  along the  $c$  axis. The observed anisotropic compression of  $\text{Ni}_2\text{Si}$  is also related to the layered structure of  $\text{Ni}_2\text{Si}$ , where hexagonal layers of  $\text{Ni}^{2+}$  cations alternate with graphite-like layers formed by  $(\text{NiSi})^{2-}$  entities. The experimental results are supported by *ab initio* total-energy calculations carried out using density functional theory and the pseudopotential method. For  $\text{Fe}_5\text{Si}_3$ , the calculations also predicted a phase transition at 283 GPa from the hexagonal  $P6_3/mcm$  phase to the cubic structure adopted by Fe and Si in the garnet  $\text{Fe}_5\text{Si}_3\text{O}_{12}$ . The room-temperature equations of state for  $\text{Fe}_5\text{Si}_3$  and  $\text{Ni}_2\text{Si}$  are also reported and a possible correlation between the bulk modulus of iron silicides and the coordination number of their minority element is discussed. Finally, we report additional descriptions of these structures, in particular, of the predicted high-pressure phase of  $\text{Fe}_5\text{Si}_3$  (the cation subarray in the garnet  $\text{Fe}_5\text{Si}_3\text{O}_{12}$ ), which can be derived from spinel  $\text{Fe}_2\text{SiO}_4$  ( $\text{Fe}_6\text{Si}_3\text{O}_{12}$ ).

DOI: [10.1103/PhysRevB.77.094113](https://doi.org/10.1103/PhysRevB.77.094113)

PACS number(s): 61.66.Fn, 62.50.-p, 64.70.K-, 71.15.Nc

### I. INTRODUCTION

The Earth's core is believed to consist of an iron-nickel alloy with several percent of light alloying elements. In particular, silicon has been suggested, from geochemical arguments, as a possible major alloying element in the Earth's outer core. On top of that, iron silicides are also considered as probable candidates of the origin of the ultralow velocity zone at the base of the Earth's mantle. These silicides may appear at the core-mantle boundary since liquid iron coexists with solid silicates. Because of these facts, the high-pressure structural stability of iron and nickel silicides is currently of interest to Earth scientists. Therefore, in order to understand the above described long-standing geophysical and geochemical subjects, a number of studies of iron silicides under pressure have been performed.<sup>1-7</sup> On the other hand, from a technological point of view, the ecologically friendly<sup>7</sup> iron and nickel silicides have also received a lot of attention since they have interesting magnetic<sup>8,9</sup> and electronic properties,<sup>10,11</sup> which make them promising candidates for optoelectronic applications<sup>10</sup> and for the development of metal-semiconductor contacts (Schottky junctions).<sup>12</sup> Finally, iron and nickel silicides are known to produce oxides in which the Fe:Si (Ni:Si) stoichiometry is maintained. Thus, the oxidation of  $\text{Fe}_5\text{Si}_3$  produces the garnet  $\text{Fe}_5\text{Si}_3\text{O}_{12}$ , whose  $\text{Fe}_5\text{Si}_3$  subarray differs from the crystal structure of the silicide itself. In the same way, the high-temperature (HT) phase of  $\text{Ni}_2\text{Si}$  ( $\theta\text{-Ni}_2\text{Si}$ ) is isostructural to the  $\text{Ni}_2\text{Si}$  subarray in the olivine-like  $\text{Ni}_2\text{SiO}_4$ . As in some cases, the cation compound of the produced oxides reproduces the structure of the high-

pressure phase of the precursor materials;<sup>13-16</sup> it has been predicted that upon compression,  $\text{Fe}_5\text{Si}_3$  is expected to undergo a phase transition to a more compact structure, which may reproduce that of the cation array in the garnet  $\text{Fe}_5\text{Si}_3\text{O}_{12}$ . Also, the room-temperature (RT) phase of  $\text{Ni}_2\text{Si}$  ( $\delta\text{-Ni}_2\text{Si}$ ) could undergo a phase transition to the  $\text{MgCu}_2$ -type structure, in the same way that  $\text{Ni}_2\text{SiO}_4$  undergoes the olivine-to-spinel phase transition. Because of the above given reasons, iron and nickel silicides are interesting compounds from geophysical, technological, and crystallochemical points of view.

In this work, we present additional studies of the high-pressure structural stability of the mineral xifengite ( $\text{Fe}_5\text{Si}_3$ ) and high-pressure structural studies of dinickel silicide ( $\text{Ni}_2\text{Si}$ ), the main component of meteoritic nickel silicide (perryite). Room-temperature angle dispersive x-ray diffraction (ADXRD) experiments were carried out in both silicides up to 75 GPa using a diamond-anvil cell (DAC). From our powder-diffraction experiments, we concluded that  $\text{Fe}_5\text{Si}_3$  remains stable in the hexagonal  $P6_3/mcm$  low-pressure phase [space group (SG) No. 193]<sup>3</sup> and  $\text{Ni}_2\text{Si}$  remains stable in the orthorhombic  $Pbnm$  structure (SG No. 62)—the  $\delta\text{-Ni}_2\text{Si}$  phase—up to the highest pressure reached in our measurements. Both structures can be seen in Figs. 1 and 2. The experimental results were complemented by *ab initio* total-energy calculations that we performed using density functional theory (DFT) and the pseudopotential method. The theoretical results not only support the experimental results, but also predict the presence beyond 283 GPa of a different denser phase in  $\text{Fe}_5\text{Si}_3$ , which has the structure adopted by

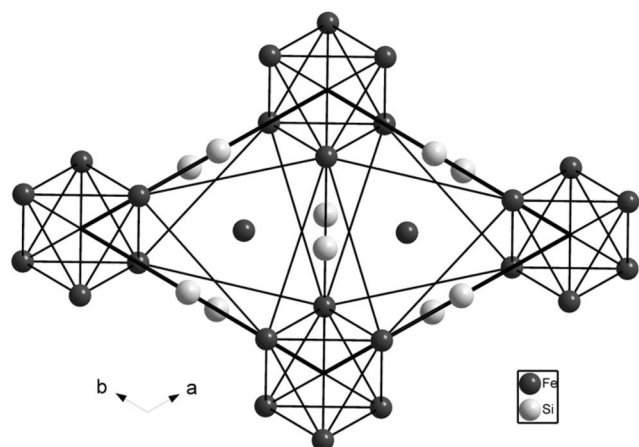


FIG. 1. The structure of  $\text{Fe}_5\text{Si}_3$  projected along the  $ab$  plane. Dark (light) circles correspond to the Fe (Si) atoms.

the  $\text{Fe}_5\text{Si}_3$  subnet in the garnet  $\text{Fe}_5\text{Si}_3\text{O}_{12}$ . Beyond this, both theory and experiment found that the  $c$  axis of  $\delta\text{-Ni}_2\text{Si}$  is much less compressible than its other two crystallographic axes. This fact is related to the bonding features of  $\delta\text{-Ni}_2\text{Si}$ . Finally, accurate RT equations of states (EOSs) for  $\text{Fe}_5\text{Si}_3$  and  $\delta\text{-Ni}_2\text{Si}$  were obtained from the experimental data and the theoretical calculations. The reported results could have important implications for the differentiation processes of the planets and the composition of their cores.

## II. EXPERIMENTAL DETAILS

The synthesis of  $\text{Fe}_5\text{Si}_3$  and  $\text{Ni}_2\text{Si}$  was performed by a solid-state reaction from stoichiometric amounts of high-purity elements. The mixture was sealed under argon in a tantalum ampoule, annealed for two days at 1223 K (well below the eutectic temperature of the system<sup>17</sup>), and then quenched by exposure to air at RT. Gray metallic dendrites were obtained. Samples were prepared as finely ground powders from the synthesized materials immediately before the loading of the DAC to minimize any possible oxidation of the silicides. The silicide dendrites were ground in a marble mortar, which contained acetone (99.99% purity), using a marble pestle. The synthesized samples were characterized by x-ray diffraction at ambient conditions. There was no indication of additional phases in the starting materials. The unit-cell parameters were  $a=6.752(5)$  Å and  $c=4.741(3)$  Å for hexagonal  $\text{Fe}_5\text{Si}_3$  and  $a=7.061(6)$  Å,  $b=4.992(4)$  Å, and  $c=3.741(2)$  Å for orthorhombic  $\delta\text{-Ni}_2\text{Si}$ , which are in excellent agreement with previous studies.<sup>3,17</sup> Several attempts to synthesize  $\text{Fe}_2\text{Si}$  were also carried out, but we were not able to obtain a pure phase. High-pressure ADXRD measurements were carried out at RT in a 300  $\mu\text{m}$  culet DAC. The powder samples were loaded together with a ruby chip into a 100- $\mu\text{m}$ -diameter hole drilled on a 200- $\mu\text{m}$ -thick rhenium gasket preindented to 35  $\mu\text{m}$ . Silicone oil was used as pressure-transmitting medium,<sup>18,19</sup> and the pressure was determined using the ruby fluorescence technique.<sup>20</sup> The ADXRD experiments were performed at the 16-IDB beam-

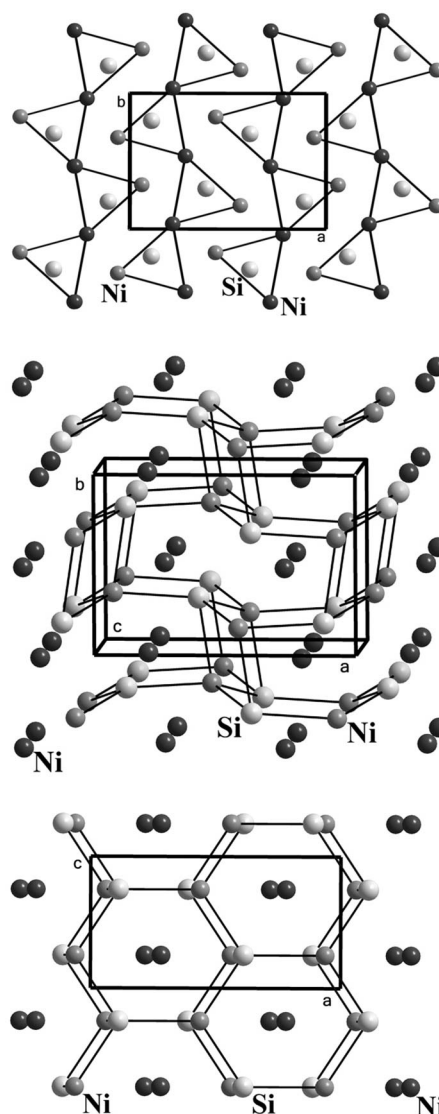


FIG. 2. The structure of  $\text{Ni}_2\text{Si}$ . (a) Projection along the  $c$  axis showing the distorted trigonal prism of Ni around the Si atoms. (b) Schematic view to show the  $\delta\text{-Ni}_2\text{Si}$  as a Ni-stuffed four coordinated net. (c) Projection along the  $b$  axis showing the presence of  $(\text{NiSi})^{2-}$  graphite-like layers. Ni and Si atoms are identified in the figure.

line of the HPCAT facility at the Advanced Photon Source (APS) using monochromatic radiation with  $\lambda=0.3931$  Å. The monochromatic x-ray beam was focused down to  $15 \times 10 \mu\text{m}^2$  by using Kickpatrick–Baez mirrors and spatially collimated with a 30  $\mu\text{m}$  molybdenum cleanup pinhole. Diffraction images were recorded with a Mar345 image plate detector, located 350 mm away from the sample, and were integrated and corrected for distortions using the FIT2D software.<sup>21</sup> A  $\text{CeO}_2$  standard was used to calibrate the detector parameters. Typical diffraction patterns were collected with 20 s exposures. Two independent runs were performed for each of the studied silicides. The indexing, structure solution, and refinements were performed using the DICVOL (Ref. 22) and POWDERCELL (Ref. 23) program packages.

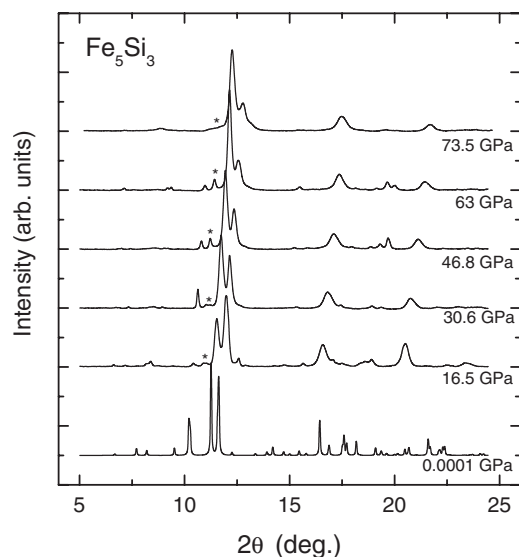


FIG. 3. Room-temperature ADXRD data of Fe<sub>5</sub>Si<sub>3</sub> at different pressures. In all diagrams, the background was subtracted. The symbols \* indicate the position of a gasket peak.

### III. OVERVIEW OF THE CALCULATIONS

The structural stability of the phases of Fe<sub>5</sub>Si<sub>3</sub>, Fe<sub>2</sub>Si, and Ni<sub>2</sub>Si was further investigated theoretically by means of total-energy calculations performed within the framework of DFT with the Vienna *ab initio* simulation package (VASP).<sup>24</sup> A review of DFT-based total-energy methods as applied to the theoretical study of phase stability can be found in Ref. 25. In the calculations, the exchange and correlation energy was described within the generalized gradient approximation described in Ref. 26. We used ultrasoft pseudopotentials and we adopted the projector augmented wave scheme. We employed a basis set of plane waves up to a kinetic energy cutoff of 334.9 eV for Fe<sub>5</sub>Si<sub>3</sub> and Fe<sub>2</sub>Si, and 336.9 eV for Ni<sub>2</sub>Si, and Monkhorst–Pack grids for the Brillouin-zone integrations which ensure highly converged and precise results [to about 1 meV/f.u.]. At each selected volume for a given structure of the considered compound, the external and internal parameters were relaxed through the calculations of the forces on the atoms and the components of the stress tensor, which yielded the values of the atomic positions and unit-cell parameters of the structure. Valuable structural information (equilibrium volume, bulk modulus, etc.) for each stable phase was obtained from the calculated energy-volume curves after a Birch–Murnaghan fitting.

## IV. RESULTS AND DISCUSSION

### A. Structural studies of Fe<sub>5</sub>Si<sub>3</sub>

Figure 3 shows our ADXRD data for Fe<sub>5</sub>Si<sub>3</sub> at several selected pressures and compares them with a diffraction pattern measured at atmospheric pressure (0.0001 GPa) outside the DAC. At ambient conditions, the obtained diffraction pattern corresponded to the hexagonal Mn<sub>5</sub>Si<sub>3</sub>-type structure (SG *P6<sub>3</sub>/mcm*, No. 193),<sup>3</sup> with no indication of any additional phase in it. Under compression, the only changes we

observed in the x-ray diffraction patterns are the typical peak broadening of DAC experiments<sup>27,28</sup> and the appearance of a peak around  $2\theta=11^\circ$ , denoted by the symbol \* in Fig. 3. This peak has been assigned to a rhenium gasket line and can be easily identified since its pressure shift is smaller than that of the Fe<sub>5</sub>Si<sub>3</sub> peaks. It is important to mention here that the gasket peak does not contaminate the x-ray diffraction pattern of Fe<sub>5</sub>Si<sub>3</sub> since it does not overlap with any of the sample peaks. Regarding the Fe<sub>5</sub>Si<sub>3</sub> peaks, we observed that they shift smoothly with compression and that all the Bragg reflections, present in the x-ray diffraction patterns, can be indexed within the *P6<sub>3</sub>/mcm* structure up to 75 GPa. The small changes of the relative intensities of some of the peaks can be assigned to preferred-orientation effects induced upon compression in the DAC.<sup>29,30</sup> From the x-ray diffraction data, we obtained the evolution with pressure of the volume and lattice parameters of Fe<sub>5</sub>Si<sub>3</sub>. We also refined the atomic positions of the Fe and Si atoms. We found that, within the pressure range of our experiments, the pressure change of the *x* coordinate of the Fe and Si atoms, located at the Wyckoff position 6g (the only two free coordinates in the structure), is smaller than the experimental uncertainty. The mean values of these coordinates are  $x_{\text{Fe}}=0.230(4)$  and  $x_{\text{Si}}=0.599(4)$ . Therefore, we concluded that the pressure effect on the atomic positions can be neglected, which is in good agreement with previous studies performed up to 30 GPa.<sup>3</sup> The pressure evolution of the unit-cell parameters of Fe<sub>5</sub>Si<sub>3</sub> is plotted in Fig. 4, where we compare them with previously reported data obtained using NaCl as pressure medium<sup>3</sup> and with our theoretical calculations. Both experiments agree within its accuracy up to 20 GPa. Beyond this pressure, the previous experiment slightly underestimates the decrease of the volume. As it has been argued in the literature,<sup>31</sup> this fact can be attributed to the larger nonhydrostatic stresses caused by the NaCl pressure medium used in the previous experiments.<sup>3</sup>

In Fig. 4, it can be seen that the contraction of the unit-cell parameters with pressure is rather isotropic. Indeed, according to our experiments, the *c/a* ratio stays nearly equal to 0.702 within the covered pressure range. The same behavior was previously observed in Ref. 3 up to 30 GPa, and our experiments verify that the compression of Fe<sub>5</sub>Si<sub>3</sub> remains isotropic up to 75 GPa. A quadratic fit to our data gives the following pressure dependence of the unit-cell parameters of Fe<sub>5</sub>Si<sub>3</sub>:

$$a = 6.76(1) - 9.5(6) \times 10^{-3}P + 3.5(7) \times 10^{-5}P^2,$$

$$c = 4.736(9) - 7.5(5) \times 10^{-3}P + 3.8(6) \times 10^{-5}P^2,$$

where *a* and *c* are given in Å and *P* is in GPa. From these two relations, it can be estimated that from atmospheric pressure up to 75 GPa *a*, and *c* are reduced approximately by 7.5%. The isotropic compression of the unit-cell parameters and the fact that the atomic positions of Fe and Si do not change upon compression suggest that the only effect of pressure in the structure of Fe<sub>5</sub>Si<sub>3</sub> is to produce a uniform change in all the bond distances as previously observed in  $\epsilon$ -FeSi.<sup>32</sup> The evolution of the bond distances of Fe<sub>5</sub>Si<sub>3</sub> with pressure has been calculated from our experimental data,

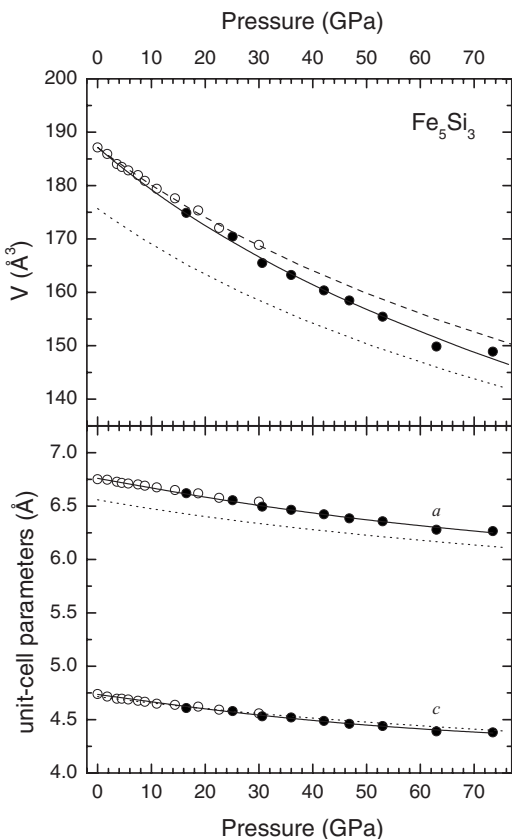


FIG. 4. Volume and lattice parameters of  $\text{Fe}_5\text{Si}_3$  under pressure. The solid circles represent the present data. The empty circles correspond to the data of Ref. 3. The solid lines are the reported EOS and quadratic fits to  $a$  and  $c$ . The dashed line represents the EOS reported in Ref. 3, and the dotted lines the theoretical results.

which is represented in Fig. 5. There, it can be seen that all the Fe-Fe and Si-Fe bonds follow a similar behavior upon compression. Additional support to this conclusion comes from the comparison of the bond distances reported at 0.0001 and 30 GPa in Ref. 3.

The present pressure-volume data shown in Fig. 4 have been analyzed using a third-order Birch–Murnaghan EOS.<sup>33</sup> By fixing the zero-pressure volume ( $V_0$ ) to its measured value ( $187.154 \text{ \AA}^3$ ), we obtained the bulk modulus ( $B_0 = 215 \pm 14 \text{ GPa}$ ) and its pressure derivative ( $B'_0 = 3.6 \pm 0.6$ ). The bulk modulus obtained from our data is 13% smaller than the value reported in Ref. 3 ( $B_0 = 243 \pm 9 \text{ GPa}$ ), but our  $B'_0$  agrees within the uncertainties with the value reported in Ref. 3 ( $B'_0 = 3.4 \pm 0.9$ ). The difference found for the bulk modulus, which is similar to the differences observed in the literature for other iron silicides,<sup>2,32,34,35</sup> may be caused by two reasons: (1) The data reported in Ref. 3 gives a smaller compressibility than the present data for  $P \geq 20 \text{ GPa}$ . (2) The Murnaghan EOS<sup>36</sup> was used in Ref. 3 to fit  $B_0$  and  $B'_0$ , and this approach usually cause an overestimation of the bulk modulus. It is important to mention here that after a comparison of the bulk modulus of  $\text{Fe}_5\text{Si}_3$  with the bulk modulus of other iron silicides reported in the literature (e.g., the different polymorphs of fersilicite,  $\text{FeSi}$ , and ferdisilicite,  $\text{FeSi}_2$ ),  $\text{Fe}_5\text{Si}_3$  seems to be the least compressible alloy. This can be

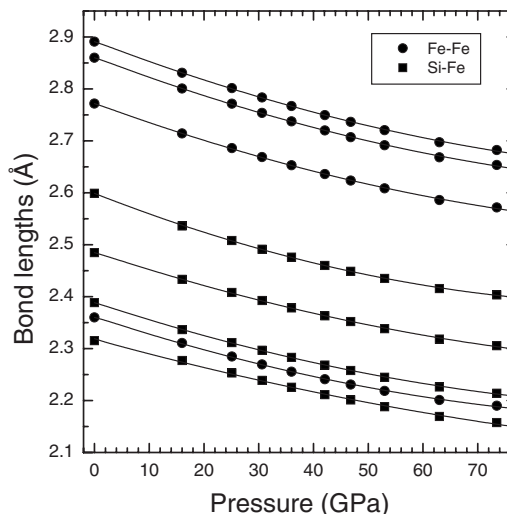


FIG. 5. Pressure dependence of the Fe-Fe and Si-Fe bond distances for the low-pressure phase of  $\text{Fe}_5\text{Si}_3$ .

seen in Table I, which summarizes the bulk modulus of different iron silicides. The compressibility of iron silicides has been previously proposed to be correlated with the coordination number (CN) of the minority element.<sup>3</sup> In the case of  $\text{Fe}_5\text{Si}_3$ , the silicon atoms have a CN=9, whereas in the other alloys,  $6 \leq \text{CN} \leq 8$ . This fact makes  $\text{Fe}_5\text{Si}_3$  the least compressible compound among the different iron silicides studied up to now. According to this hypothesis, the hypothetical high-pressure phase of  $\text{Fe}_5\text{Si}_3$  (the garnet-like), which has a CN=10, and  $\text{Fe}_2\text{Si}$ , which has a CN=11, should have a bulk modulus larger than 240 GPa. As we will show in the following, this is exactly what we have obtained from our *ab initio* calculations.

We compare now the experimental data presented with the results obtained from our total-energy calculations. Fig-

TABLE I. Bulk modulus and coordination number of the minority element in different iron silicides.

Compound	$B_0$ (GPa)	CN of minority element	Reference
$\alpha\text{-FeSi}_2$	167	6	39
$\alpha\text{-FeSi}_2$	172–182	6	37 and 39
$\text{Fe}_3\text{Si}$	182	7	39
$\varepsilon\text{-FeSi}$	160–200	7	32 and 33
$\text{CsCl-FeSi}$	184–225	8	37 and 40
$\beta\text{-FeSi}_2$	180–200	8	34 and 38
$\text{Fe}_7\text{Si}_3$	199–207	8	2 and 5
hex- $\text{Fe}_5\text{Si}_3$	$215 \pm 14$	9	This work (experimental)
hex- $\text{Fe}_5\text{Si}_3$	239	9	This work (calculated)
hex- $\text{Fe}_5\text{Si}_3$	$243 \pm 9$	9	3
cubic- $\text{Fe}_5\text{Si}_3$	250	10	This work (calculated)
$\text{Fe}_2\text{Si}$	255	11	This work (calculated)

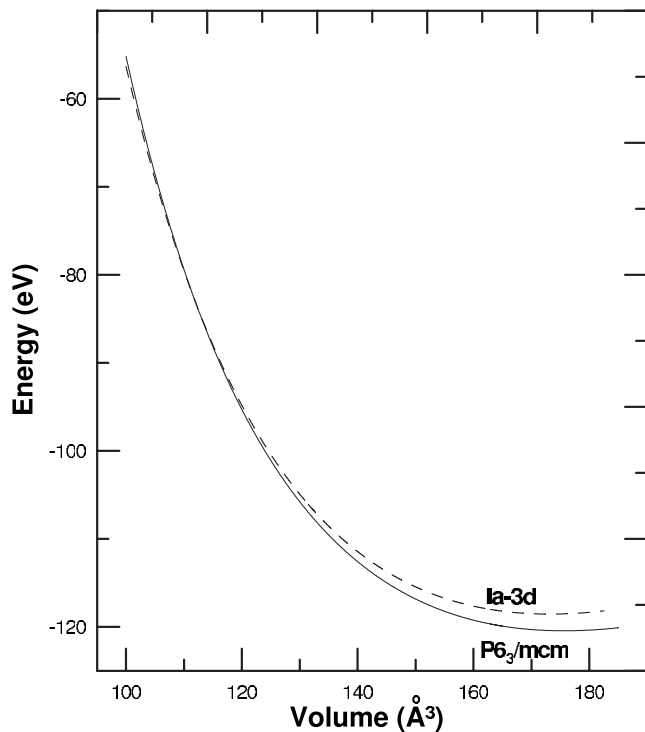


FIG. 6. Total-energy versus volume from *ab initio* calculations for the analyzed structures of Fe<sub>5</sub>Si<sub>3</sub>. Only the most competitive structures are shown. (Volume and energy are 2 f.u.).

Figure 6 shows the energy-volume curves for the different structures considered for Fe<sub>5</sub>Si<sub>3</sub>, from which the relative stability of the different phases can be extracted. Based on either crystallochemical arguments or in its present observation in compounds related to Fe<sub>5</sub>Si<sub>3</sub>, we have considered the following structures in our calculations: hexagonal Mn<sub>5</sub>Si<sub>3</sub> type (SG *P6<sub>3</sub>/mcm*, No. 193),<sup>3</sup> tetragonal Eu<sub>5</sub>Si<sub>3</sub> type (SG *I4/mcm*, No. 140),<sup>41</sup> orthorhombic Sr<sub>5</sub>Sb<sub>3</sub> type (SG *Pnma*, No. 62),<sup>42</sup> and cubic *Ia $\bar{3}d$*  (SG No. 230).<sup>3</sup> For the sake of clarity, only the most competitive structures are shown in Fig. 6. This figure shows the hexagonal *P6<sub>3</sub>/mcm* structure to be stable up to 283 GPa, which agrees with the absence of phase transitions observed in the experiments up to 75 GPa. In addition, from the calculations, we obtained the following EOS parameters for the *P6<sub>3</sub>/mcm* structure:  $V_0=175.7 \text{ \AA}^3$ ,  $B_0=238.76 \text{ GPa}$ , and  $B'_0=3.8 \text{ GPa}$ . These values compare well with the experimental results, with differences within the typical reported systematic errors in DFT calculations. A similar degree of agreement exists for the calculated values of the internal parameters  $x_{\text{Fe}}=0.2450$  for the Fe (6g) atoms and  $x_{\text{Si}}=0.6044$  for the Si (6g) atoms (experimental: 0.230 and 0.599, respectively), and  $c/a$  ratio=0.719 (experimental: 0.702). The differences between the calculated volume and axial ratio can be mainly caused by an underestimation of the lattice parameter  $a$  by 3% (see Fig. 4). However, the calculated pressure evolution of  $a$  follows a very similar trend as the experimental results. Our calculations also confirm that the compression of Fe<sub>5</sub>Si<sub>3</sub> is isotropic up to 283 GPa, i.e., in the whole range of stability of the hexagonal phase of Fe<sub>5</sub>Si<sub>3</sub>. Based on The calculations, there is no important effect of the

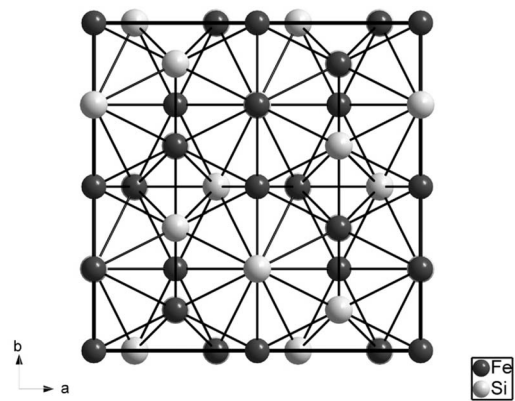


FIG. 7. The structure of Fe<sub>2</sub>Si projected in the  $ab$  plane. Dark (light) circles correspond to the Fe (Si) atoms.

pressure on the atomic positions of Fe and Si, in good agreement with our experiments.

As pressure increases, according to our calculations, the hexagonal *P6<sub>3</sub>/mcm* structure becomes unstable and converts into a body-centered-cubic phase (SG *Ia $\bar{3}d$* , No. 230) with Fe<sub>1</sub> and Fe<sub>2</sub> atoms at 24c and 16a positions, respectively, and the Si atoms at the 24d sites (see Fig. 7). This high-pressure phase is isomorphous to the structure adopted by the Fe<sub>5</sub>Si<sub>3</sub> subarray in the Fe<sub>5</sub>Si<sub>3</sub>O<sub>12</sub> garnet. This fact is in full agreement with the hypothesis that proposes the existence of a correlation between oxidation and pressure.<sup>14,15</sup> The high-pressure phase only emerges as thermodynamically stable above a compression threshold of about 283 GPa. From the common tangent construction or the enthalpy versus pressure plot,<sup>25</sup> our calculations predict that Fe<sub>5</sub>Si<sub>3</sub> becomes unstable in the *P6<sub>3</sub>/mcm* phase at 283 GPa against the cubic *Ia $\bar{3}d$*  phase. The transition is a first-order phase transition with a volume change of 1.1% and implies an increase of the Si coordination. The Si atoms (minority element) are coordinated by nine Fe atoms in the low-pressure phase and by ten Fe atoms in the high-pressure phase. The EOS fitting to the theoretical results gives  $V_0=346.60 \text{ \AA}^3$ ,  $B_0=249.95 \text{ GPa}$ , and  $B'_0=3.77$  for the predicted high-pressure phase. This EOS, indeed, confirms that an increase of the coordination number of the minority element of the alloy should imply an increase of the bulk modulus.

In order to further check this hypothesis, we have also performed *ab initio* total-energy calculations for Fe<sub>2</sub>Si. For this alloy, two different polymorphs have been reported in the literature, the cubic hapekite structure (SG *Pm $\bar{3}m$* , No. 221),<sup>43</sup> found in grains of lunar meteorites, and a trigonal structure (SG *P $\bar{3}m1$* , No. 164),<sup>44</sup> which is a slight distortion of the Ni<sub>2</sub>Al-type structure. According to our calculations, at zero and low pressure, the most stable structure for Fe<sub>2</sub>Si is the trigonal structure reported by Kudielka,<sup>44</sup> with the cubic hapekite structure being higher in energy by more than 200 meV/f.u. Regarding the trigonal structure of Fe<sub>2</sub>Si, we also found that in this structure, which we will name  $\alpha$ -Fe<sub>2</sub>Si, the three crystallographically independent Fe atoms are located at the 1a (0, 0, 0), 1b (0, 0,  $\frac{1}{2}$ ), and 2d ( $\frac{1}{3}$ ,  $\frac{2}{3}$ , 0.73) sites, and the Si atoms at 2d ( $\frac{1}{3}$ ,  $\frac{2}{3}$ , 0.25) sites, in good agree-

TABLE II. Structural parameters of  $\text{Fe}_2\text{Si}$ . Data taken from Ref. 44. space group  $P\bar{3}m1$ ,  $a=4.052 \text{ \AA}$ , and  $c=5.085 \text{ \AA}$ .

Atom	Site	$x$	$y$	$z$
$\text{Fe}_1$	$1a$	0	0	0
$\text{Fe}_2$	$1b$	0	0	0.5
$\text{Fe}_3$	$2d$	1/3	2/3	0.78
$\text{Si}_1$	$2d$	1/3	2/3	0.28

ment with the experimental data<sup>44</sup> (see Table II). It is important to note that in  $\alpha\text{-Fe}_2\text{Si}$ , the Si atoms (the minority element) are coordinated by 11 Fe atoms. The EOS fit to our theoretical results for  $\alpha\text{-Fe}_2\text{Si}$  gives  $V_0=64.985 \text{ \AA}^3$ ,  $B_0=255 \text{ GPa}$ , and  $B'_0=3.8$ . The obtained axial ratio for this structure is  $c/a=1.245$ . The calculated ambient pressure-volume underestimates the measured value of  $72.3 \text{ \AA}^3$ , but the difference is within the typical systematic errors of DFT calculations. The calculated axial ratio is in very good agreement with the experimental value (1.255). Regarding the compressibility of  $\alpha\text{-Fe}_2\text{Si}$ , our calculations show that this silicide has a large bulk modulus, 2% larger than that of the high-pressure phase of  $\text{Fe}_5\text{Si}_3$ , which gives additional support to the idea that relates the bulk modulus with the coordination number of the minority element in iron silicides.

### B. Structural studies of $\delta\text{-Ni}_2\text{Si}$

At atmospheric pressure, the obtained diffraction pattern for  $\text{Ni}_2\text{Si}$  corresponded to the orthorhombic  $Pbnm$  structure ( $\delta\text{-Ni}_2\text{Si}$ ), with no indication of any extra phase in it. Under compression, we observed that all the  $\text{Ni}_2\text{Si}$  peaks shift smoothly with compression and that all of them can be assigned to the  $Pbnm$  structure up to 75 GPa. From our x-ray diffraction data, we obtained the evolution with pressure of the volume and lattice parameters. We also obtained the atomic positions, with the Ni atoms being located at two different  $4c$  sites of coordinates (0.063, 0.325, 0.25) and (0.203, 0.042, 0.75), respectively, and the Si atoms also at  $4c$  with coordinates (0.386, 0.263, 0.25). These positions agree with those reported in the literature<sup>17</sup> and the effect of pressure on them is comparable with the uncertainty of the experiments. The pressure dependences of the lattice parameters and the volume of  $\text{Ni}_2\text{Si}$  are plotted in Fig. 8. The present pressure-volume data have been analyzed using a third-order Birch–Murnaghan EOS.<sup>33</sup> By fixing  $V_0$  to its measured value ( $131.049 \text{ \AA}^3$ ), we obtained  $B_0=167 \pm 5 \text{ GPa}$  and  $B'_0=4.5 \pm 0.5$ . The obtained bulk modulus is very similar to that of  $\varepsilon\text{-Fe}$  ( $B_0=163.4 \pm 7.9 \text{ GPa}$  and  $B'_0=5.38 \pm 0.16$ ), which the stable phase of iron at Earth's core conditions.<sup>45</sup>  $\text{Ni}_2\text{Si}$  is known to have at atmospheric pressure a density ( $\rho$ ) of  $7.2 \text{ g/cm}^3$  and a melting temperature ( $T_M$ ) of 1600 K. These values are close to those of pure iron,  $\rho=7.8 \text{ g/cm}^3$  and  $T_M=1810 \text{ K}$ .<sup>46</sup> Based on these facts and the common presence of  $\text{Ni}_2\text{Si}$  in meteorites, it has been speculated that nickel disilicide could be present in the core of the Earth.<sup>47</sup> As we will show later, our calculations suggest that  $\text{Ni}_2\text{Si}$  remains stable in the orthorhombic  $Pbnm$  structure at

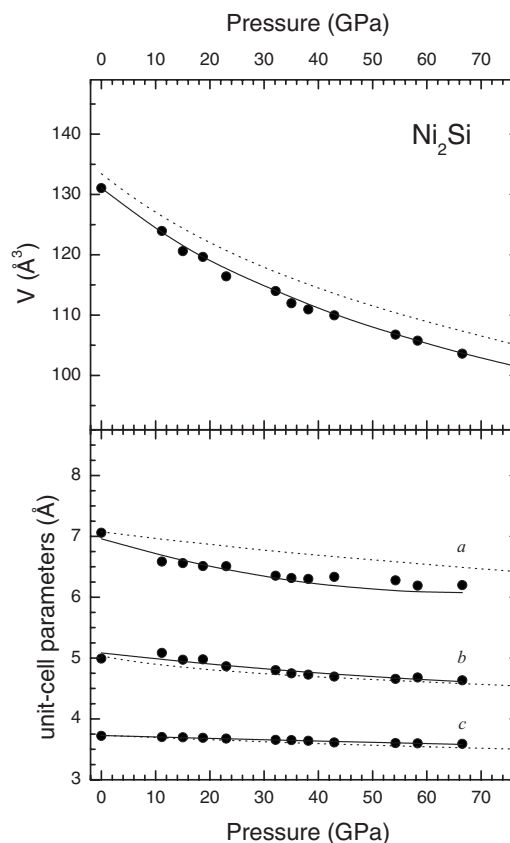


FIG. 8. Volume and lattice parameters of  $\text{Ni}_2\text{Si}$  under pressure. The solid circles represent the present data. The solid lines are the reported EOS and quadratic fits to  $a$ ,  $b$ , and  $c$ , and the dotted lines the theoretical results.

Earth's inner core pressures. According to the present results, even at such extreme pressures, the difference between the density of  $\delta\text{-Ni}_2\text{Si}$  and  $\varepsilon\text{-Fe}$  stays close to 10%.

In Fig. 8, it can be seen that the contraction of the unit-cell parameters with pressure is highly anisotropic. In particular, the  $c$  axis is much less compressible than the other two crystalline axes. A quadratic fit to our data reported in Fig. 8 gives the following pressure dependence of the unit-cell parameters of  $\text{Ni}_2\text{Si}$ :

$$a = 7.00(5) - 2.6(6) \times 10^{-2}P + 2.0(3) \times 10^{-4}P^2,$$

$$b = 5.085(9) - 1.0(3) \times 10^{-2}P + 4(1) \times 10^{-5}P^2,$$

$$c = 3.278(6) - 2.4(4) \times 10^{-3}P + 3.6(9) \times 10^{-6}P^2,$$

where  $a$ ,  $b$ , and  $c$  are given in  $\text{Å}$  and  $P$  is given in GPa. From these three relations, it can be estimated that from atmospheric pressure up to 75 GPa,  $a$  is reduced by 12.7%,  $b$  is reduced by 9.3%, and  $c$  is reduced by 3.9%. From these results, it can also be deduced that the linear incompressibility of  $\delta\text{-Ni}_2\text{Si}$  along the  $c$  axis is 1450 GPa, i.e., it is similar to the linear incompressibility of diamond. This unique mechanical property would make  $\delta\text{-Ni}_2\text{Si}$  suitable for technological applications under extreme conditions. A better understanding of the observed anisotropic compressibility can

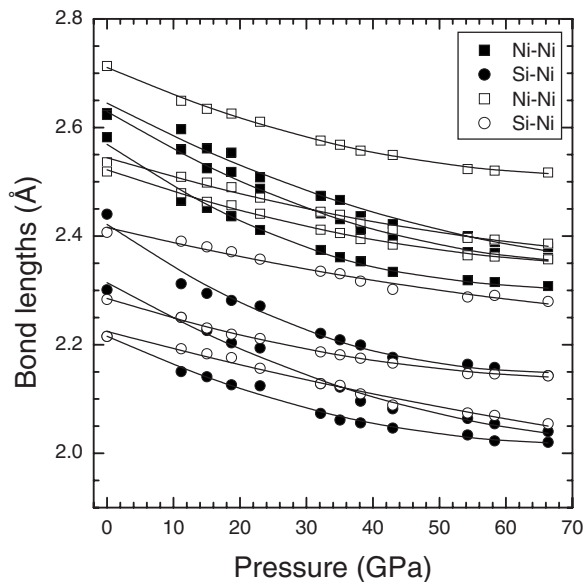


FIG. 9. Pressure dependence of the Ni-Ni and Si-Ni bond distances for Ni<sub>2</sub>Si. The empty (solid) symbols represent the bonds orientated along (perpendicular to) the *c* axis. The lines are quadratic fits to the experimental data.

be obtained from the analysis of the pressure evolution of the interatomic bond distances. We calculated the Ni-Ni and Ni-Si bond distances from our experimental data. The obtained results as a function of pressure are shown in Fig. 9. There, it can be seen that the atomic bonds that are mainly oriented perpendicular to the *c* axis (solid symbols) are much more compressible than the atomic bonds oriented along the *c* axis (empty symbols). This fact can be related to the anisotropic valence-electron density of Ni<sub>2</sub>Si, mostly distributed along the *c* axis.<sup>48</sup> This suggests that the directionality of the valence-electron density is responsible for the large incompressibility of the *c* axis of Ni<sub>2</sub>Si.

This large incompressibility can also be understood by observing the structure represented in Fig. 2. When projected along the *c* axis [Fig. 2(a)], one sees the classical description of  $\delta$ -Ni<sub>2</sub>Si in terms of zigzag chains of Ni<sub>6</sub>Si trigonal prisms, further connected by edge sharing to form blocks perpendicular to the *a* axis.<sup>49</sup> However, in a recent reinterpretation of this structure type,<sup>50</sup> the  $\delta$ -Ni<sub>2</sub>Si structure has been described as a Ni-stuffed, four-connected net, typical of the group 14 elements [see Fig. 2(b)]. This structure is formed by puckered layers of hexagonal rings with some additional bonds between them. Within this framework, the structure of  $\delta$ -Ni<sub>2</sub>Si can be thought of as being formed by alternating hexagonal layers of Ni<sup>2+</sup> cations perpendicular to the *b* axis, and graphite-like layers perpendicular to the *b* axis formed by (NiSi)<sup>2-</sup> entities [see Fig. 2(c)]. This layered characteristic of  $\delta$ -Ni<sub>2</sub>Si could be responsible for the observed difference of compressibility among different directions in Ni<sub>2</sub>Si, as observed in other layered crystals such as InSe (Ref. 51) or ReB<sub>2</sub>.<sup>52</sup>

We compare now the experimental data presented here with the results from our total-energy calculations. Figure 10 shows the energy-volume curves for most relevant structures

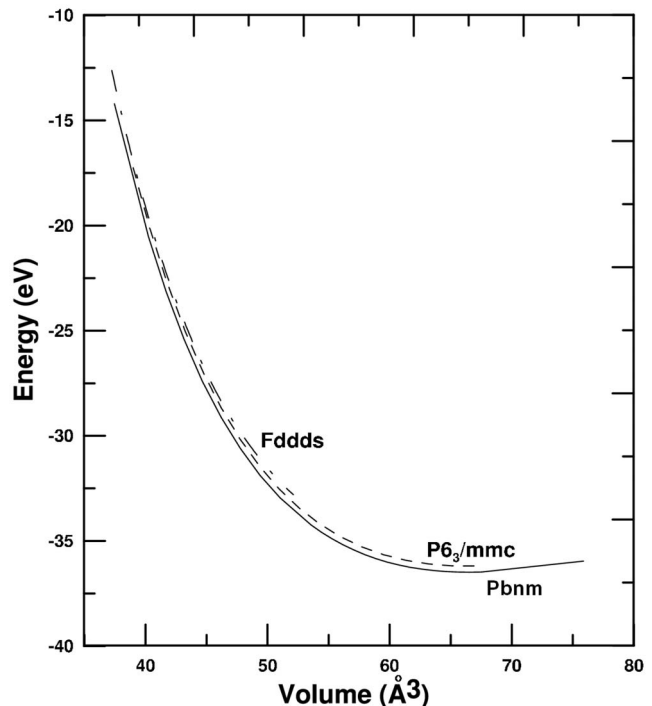


FIG. 10. Total-energy versus volume from *ab initio* calculations for the analyzed structures of Ni<sub>2</sub>Si. Only the most competitive structures are shown. (Volume and energy are 2 f.u.).

among the several structures considered for Ni<sub>2</sub>Si. From it, the relative stability of the different phases can be extracted. In order to theoretically test the structural stability of Ni<sub>2</sub>Si, in addition to the  $\delta$ -Ni<sub>2</sub>Si and  $\theta$ -Ni<sub>2</sub>Si structures, we have selected some candidate structures adopted by other A<sub>2</sub>X compounds. These structures include the Si<sub>2</sub>Ti-type structure (SG *Fddd*, No. 70),<sup>53</sup> the Ni<sub>2</sub>In-type structure (SG *P6<sub>3</sub>/mmc*, No. 194),<sup>54</sup> and the MgCu<sub>2</sub>-type structure (SG *Fd $\bar{3}m$* , No. 227),<sup>55</sup> also known as the Cubic Laves phase (*C15* structure). Figure 10 shows the orthorhombic *Pbnm* structure to be stable up to nearly 400 GPa (the maximum pressure studied in our theoretical calculations), which agrees with the absence of phase transitions observed in the experiments up to 75 GPa. Our calculations also confirm that the compression of Ni<sub>2</sub>Si is highly anisotropic, with the *c* axis being the less compressible axis (see Fig. 8). In addition, the calculations give for the *Pbnm* structure of Ni<sub>2</sub>Si the following EOS parameters:  $V_0=133.44 \text{ \AA}^3$ ,  $B_0=175.07 \text{ GPa}$ , and  $B'_0=5$ . The theoretically calculated EOS is shown together with the experimental data in Fig. 8. There, it can be seen that, in spite of the systematic volume overestimation, the *ab initio* calculations give a very similar compressibility as the experiments. The overestimation of the volume comes principally from the overestimation of the value of the unit-cell parameter *a*. The calculated values of the internal parameters agree also very well with the experimental values  $x_{\text{Ni1}}=0.0606$ ,  $y_{\text{Ni1}}=0.3304$ ,  $x_{\text{Ni2}}=0.2039$ ,  $y_{\text{Ni2}}=0.0404$ , and  $x_{\text{Si}}=0.3855$ ,  $y_{\text{Si}}=0.2862$  for the 4*c* Ni and Si atoms.

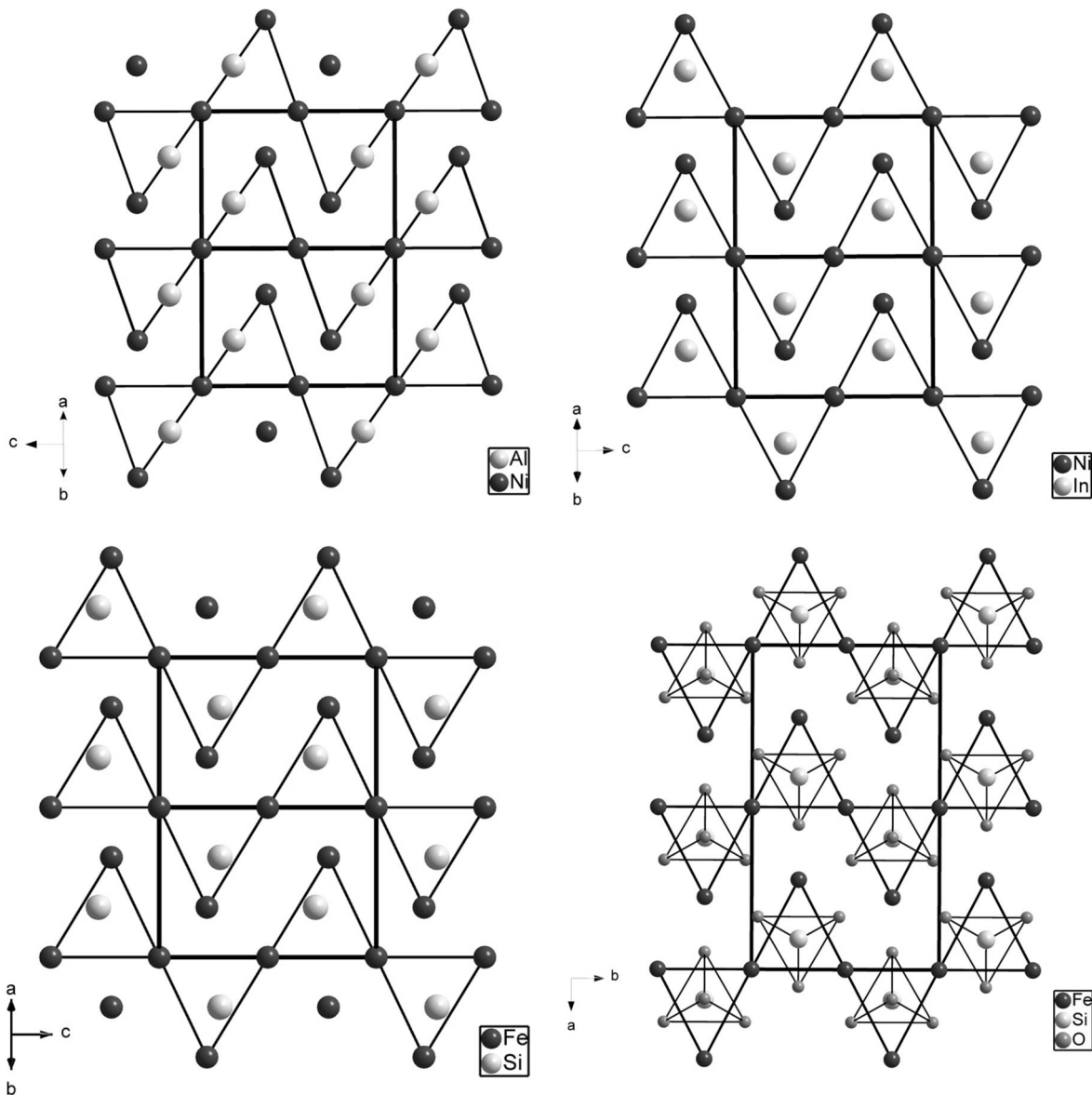


FIG. 11. The structures of (a)  $\text{Ni}_2\text{Al}$ , (b)  $\text{Ni}_2\text{In}$ , (c)  $\text{Fe}_2\text{Si}$ , and (d)  $\text{Fe}_2\text{SiO}_4$ . Different atoms are identified in the figure.

## V. CRYSTAL CHEMISTRY OF $\text{Fe}_5\text{Si}_3$ , $\text{Fe}_2\text{Si}$ , AND $\text{Ni}_2\text{Si}$

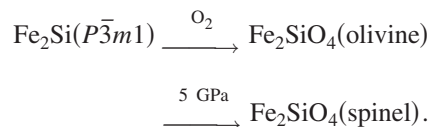
### A. $\text{Fe}_2\text{Si}$ , $\text{Ni}_2\text{Si}$ , and the related oxides olivine and spinel $\text{Fe}_2\text{SiO}_4$

The only reference to the synthesis and structure elucidation of  $\text{Fe}_2\text{Si}$  ( $P\bar{3}m1$ ) was published by Kudielka.<sup>44</sup> As seen in Figs. 11(a)–11(c), the reported structure is in between the  $\text{Ni}_2\text{Al}$ -type and the  $\text{Ni}_2\text{In}$ -type structures. From this figure, it could be concluded that the  $\text{Ni}_2\text{Al}$ -type structure could transform into the  $\text{Ni}_2\text{In}$  type by a continuous displacement of both  $\text{Fe}_3$  and  $\text{Si}$  atoms. This fact could be related to the fact that theoretical calculations encounter some problems in determining which of the three structures (trigonal,  $\text{Ni}_2\text{Al}$  type or  $\text{Ni}_2\text{In}$  type) is the most stable in  $\text{Fe}_2\text{Si}$ . In particular, in the relaxation of these phases, we found the existence of a number of local minima. These structurally different minima are located very close in energy, sometimes separated by shallow

barriers, which make the precise determination of the absolute minimum within this set of crystal structures a rather tedious and difficult task. Indeed, theoretical calculations starting from the atomic coordinates reported for  $\text{Fe}_2\text{Si}$  could converge upon compression to the structural parameters of either  $\text{Ni}_2\text{Al}$  type or  $\text{Ni}_2\text{In}$  type, with the former being the most stable structure among these two. The lattice parameters of  $\text{Fe}_2\text{Si}$  are given in Table II. When the  $z$  coordinates of both  $\text{Fe}_3$  and  $\text{Si}$  atoms become  $\frac{2}{3}$  and  $\frac{1}{6}$ , respectively, the  $\text{Ni}_2\text{Al}$ -type structure is produced. When fixed at  $\frac{3}{4}$  and  $\frac{1}{4}$ , respectively, the  $\text{Ni}_2\text{In}$ -type ( $P6_3/mmc$ ) structure is formed.

The important issue here is that the  $\text{Fe}_2\text{Si}$  structure is very close to the  $\text{Ni}_2\text{In}$  type, which is the  $\text{Fe}_2\text{Si}$  array existing in the olivine-like  $\text{Fe}_2\text{SiO}_4$  [see Fig. 11(d)], as was pointed out earlier.<sup>3</sup> That means that when oxygen is inserted, the  $\text{Ni}_2\text{In}$ -type structure remains in the oxide, as in many other alloys.<sup>14,15</sup> Thus, the following transitions can be observed

either by inserting oxygen<sup>14</sup> or increasing pressure.<sup>56</sup>

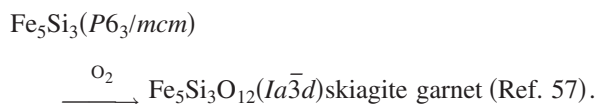
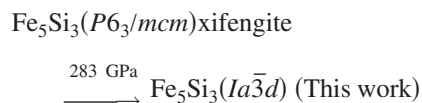


The unsolved problem is, however, that the transformation Ni<sub>2</sub>In-type-to-MgCu<sub>2</sub>-type that occurs in the oxides, as the olivine-to-spinel transition, cannot be predicted for the Fe<sub>2</sub>Si alloy in the pressure range covered by this work. This transition, which, as far as we know, has never been observed in alloys, should occur, for Fe<sub>2</sub>Si (also for Ni<sub>2</sub>Si), at extremely high pressures.

As mentioned above, we tried the synthesis of Fe<sub>2</sub>Si, but the impossibility of obtaining a pure phase led us to substitute this compound with the related Ni<sub>2</sub>Si. This compound, reported by Toman,<sup>17</sup> is dimorphous. At RT, it is of the Co<sub>2</sub>Si type ( $\delta$ -Ni<sub>2</sub>Si), being strongly related to cotunnite, but at HT it transforms into the Ni<sub>2</sub>In-type structure ( $\theta$ -Ni<sub>2</sub>Si). Although the corresponding oxide Ni<sub>2</sub>SiO<sub>4</sub> (olivine-like) undergoes the olivine-to-spinel transition, the corresponding transition in the alloy to the MgCu<sub>2</sub>-type structure could not be observed up to 75 GPa. Theoretical calculations carried out in this work indicate that, even up to 400 GPa, this transition does not take place.

### B. Fe<sub>5</sub>Si<sub>3</sub> and the garnet Fe<sub>5</sub>Si<sub>3</sub>O<sub>12</sub>

The three compounds studied here are related from a crystal chemical point of view. The structural behavior of the Fe<sub>5</sub>Si<sub>3</sub> and its related oxide, the garnet Fe<sub>5</sub>Si<sub>3</sub>O<sub>12</sub>, is summarized below:



The structure of xifengite is presented in Fig. 1, projected on the *ab* plane. It belongs to the Mn<sub>5</sub>Si<sub>3</sub> type and is also adopted by several cation arrays, such as Ca<sub>5</sub>P<sub>3</sub> in apatite (Ca<sub>5</sub>P<sub>3</sub>O<sub>12</sub>F).

In this paper, however, the description will focus on other aspects, such as the coordination polyhedron of the Fe atoms around the Si atoms, because the CN normally increases with pressure. As seen in Table I, this feature is helpful in rationalizing the bulk modulus found for the different phases of iron silicides. In Fe<sub>5</sub>Si<sub>3</sub>, the Si atoms are surrounded by nine Fe atoms, forming a polyhedron, which can be seen as a distorted square antiprism, with an additional Fe atom capping one of the square faces.

As discussed above, theoretical calculations predict that, at 283 GPa, the silicide xifengite transforms into a cubic structure that coincides with the cation array of the garnet Fe<sub>5</sub>Si<sub>3</sub>O<sub>12</sub> (skiaigite).<sup>57</sup> Because the garnet structure is rather

TABLE III. Atomic coordinates for the high-pressure phase of Fe<sub>5</sub>Si<sub>3</sub> and the garnet Fe<sub>5</sub>Si<sub>3</sub>O<sub>12</sub>. Both compounds are cubic (space group *Ia* $\bar{3}$ *d*) with lattice parameters  $a=7.02 \text{ \AA}$  and  $a=11.73 \text{ \AA}$ , respectively.

Atom	Site	<i>x</i>	<i>y</i>	<i>z</i>
O (garnet)	96 <i>h</i>	0.03529	0.05288	0.65769
Fe <sub>1</sub>	24 <i>c</i>	0.125	0	0.25
Fe <sub>2</sub>	16 <i>a</i>	0	0	0
Si	24 <i>d</i>	0.375	0	0.25

complicated, we see a necessary comprehensive description of this oxide. Both compounds, the alloy Fe<sub>5</sub>Si<sub>3</sub> ( $P > 283 \text{ GPa}$ ) and the oxide Fe<sub>5</sub>Si<sub>3</sub>O<sub>12</sub>, are cubic (*Ia* $\bar{3}$ *d*,  $Z=8$ ), with unit-cell parameters  $a=7.02 \text{ \AA}$  and  $a=11.73 \text{ \AA}$ , respectively. Their atomic coordinates are given in Table III.

The classical description of the garnet structure can be found in textbooks devoted to structural chemistry.<sup>58</sup> This description emphasizes the cation-centered, oxygen coordination polyhedra. Thus, Si atoms form isolated tetrahedral orthosilicate groups (SiO<sub>4</sub>). The Fe atoms occupy two crystallographically independent positions and have two different coordination polyhedra. Fe<sub>2</sub> are at the center of O octahedra and the Fe<sub>1</sub> atoms are surrounded by eight O atoms, forming a rather distorted cube. Its crystal chemical notation would be Fe<sup>[8]</sup><sub>3</sub>Fe<sup>[6]</sup><sub>2</sub>Si<sup>[4]</sup><sub>3</sub>O<sub>12</sub>. This simple description was considered unsatisfactory by O'Keeffe and Hyde<sup>59</sup> in their alternative approach, describing crystal structures as oxygen-stuffed alloys.

These authors noticed that the cation array of the garnet-like structure was related to that of the Cr<sub>3</sub>Si alloy. Both structures are presented in Fig. 12. In Fig. 12(a), we have drawn a complete unit cell ( $a=4.55 \text{ \AA}$ ) of the Cr<sub>3</sub>Si structure ( $Pm\bar{3}n$ ,  $Z=2$ ).<sup>60</sup> It is formed by a body-centered-cubic (bcc) array of Si atoms whose faces are centered by pairs of Cr atoms separated at short distances of  $2.27 \text{ \AA}$ . The 12 Cr atoms, when connected, form an irregular icosahedron centered by the Si atom. In Fig. 12(b), it is represented as 1/8 of the unit cell of the garnet Fe<sub>5</sub>Si<sub>3</sub>O<sub>12</sub> ( $a=11.73 \text{ \AA}$ ). As seen, both structures are topologically identical. In the case of the oxide, the unit cell is doubled because both Fe<sub>1</sub> and Si atoms alternate at the face centers. It must be outlined that *Ia* $\bar{3}$ *d* becomes a subgroup of the type IIa by doubling the unit cell of the SG  $Pm\bar{3}n$ . On the contrary, here, the bcc array is formed by the Fe<sub>2</sub> atoms. It can be concluded that the similarities between both compounds are merely topological, but that the atomic species and, hence, the superstructure formed in the oxide must obey significant chemical differences. In connection with this, it is worth remarking that the center of the icosahedrons are occupied in both compounds by an isolated atom (Si and Fe<sub>2</sub>, respectively), in spite of being the biggest hole in the structure (CN 12). On the contrary, in skiaigite, the faces are centered by SiO<sub>4</sub> groups, instead of the Cr atoms of the compound.

However, it has been outlined elsewhere<sup>14,15</sup> that the alloys described in Ref. 59 are mostly nonexistent and that an

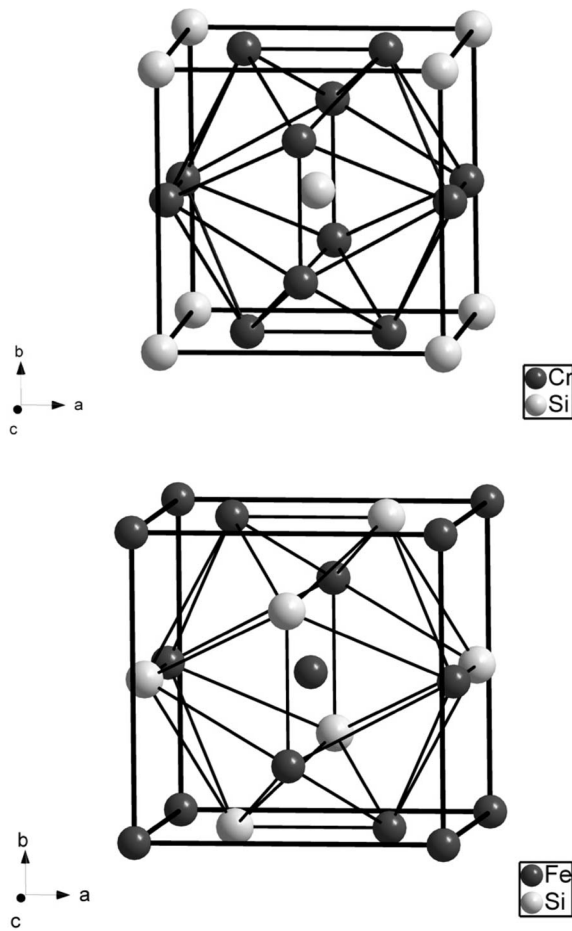


FIG. 12. The structure of (a)  $\text{Cr}_3\text{Si}$  and (b) the cation subarray of garnet  $\text{Fe}_2\text{SiO}_4$ . Different atoms are identified in the figure.

extension of their approach, based on real stuffed alloys, was further proposed by Vegas and Jansen.<sup>14,15</sup> As said in the Introduction, this study was undertaken in part as an additional proof of this approach. Our theoretical calculations predict the xifengite-to-garnet-like transition at high pressure. The structure of the high-pressure iron silicide is identical to the same array in the garnet. Thus, this is a different example of a *real* oxygen-stuffed alloy.

A question which arises from the above discussion is why the Si and Fe atoms interchange their role in both com-

pounds. This problem, which could not be solved by a simple topological comparison of both structures  $\text{Cr}_3\text{Si}$  and  $\text{Fe}_5\text{Si}_3\text{O}_{12}$ , could find a solution by comparing the garnet structure with other related iron silicates, such as  $\text{Fe}_2\text{SiO}_4$ .

It is well known that  $\text{Fe}_2\text{SiO}_4$  (olivine-like at ambient pressure) transforms into the spinel structure at 5 GPa.<sup>56</sup> Following O’Keeffe and Hyde,<sup>59</sup> the  $\text{Fe}_2\text{Si}$  array in spinels ( $\text{MgCu}_2$  type) can be seen as a three-dimensional network of Fe tetrahedral arrays, sharing all corners. This array corresponds to one-half of the atoms forming a face-centered-cubic structure and the missing atoms originating big voids, which are truncated tetrahedra formed by 12 Fe atoms and where the Si atoms ( $\text{SiO}_4$  groups) are located. One of these truncated tetrahedra is presented in Fig. 13(a). In the high-pressure transition, the Si atoms increase their CN from 11 (in olivine) to 12 (in spinel). Another interesting aspect of the spinel structure is that the Si atoms alone form a diamond-like (really a Si-like) network in spite of being formed by isolated orthosilicate groups.

Once we have described the cation array in the spinel structure, we are in the condition of establishing a different structural relationship with that of garnet. Their relation is better deduced if we put their formula on the same basis:

$$\text{Fe}_6\text{Si}_3\text{O}_{12}(\text{spinel}) - \text{Fe}_5\text{Si}_3\text{O}_{12}(\text{garnet}).$$

By looking at the formulas, we could convert the spinel structure into the garnet structure by only eliminating 1/6 of the Fe atoms. The important question, here, is whether the elimination of one Fe atom can be considered as a mere *gedanken experiment*, which makes the two compounds have almost the same empirical formula or, on the contrary, this small change in composition only produces, proportionally, small changes in the structure. If this were so, then the garnet structure must preserve important similarities with the structure of spinel. The answer to this crucial question is that both structures are strongly related.

We discussed above that the Fe atoms, in spinel, form a three-dimensional (3D) network of corner-connected tetrahedra. In the garnet structure, however, the Fe atoms form a 3D network of trigonal bipyramids (two tetrahedra with a common base), whose corners are all shared with adjacent bipyramids. Thus, as a consequence of the lower Fe contents, the tetrahedra condense in denser groups. This condensation also produces, however, big voids which are not anymore the

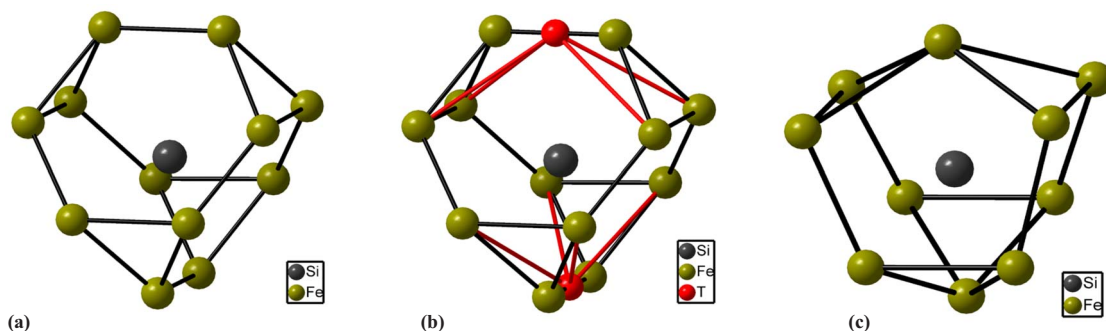


FIG. 13. (Color online): Relationship between the (a) spinel and (b) garnet polyhedra. The dark (light) circles represent the Fe (Si) atoms. The Fe atom migrating to the center of the edges to produce the garnet polyhedron are shown in red.

truncated tetrahedron presented in Fig. 13(a), but a different polyhedron formed by ten Fe atoms. As expected, the CN decreases from 12 to 10. Like in spinel, the SiO<sub>4</sub> groups are also located at the center of these voids. The differences are well illustrated in Fig. 13. In Fig. 13(a) is drawn the truncated tetrahedron (12 Fe atoms) of spinels and in Fig. 13(c), we have presented the different polyhedron formed in garnets. The transition between them can be achieved by eliminating one of the two atoms involved in opposite edges of Fig. 13(a). When these two atoms disappear, the two remaining Fe atoms migrate to the center of the edges, so producing the polyhedron of the garnet. These Fe (migrated) atoms have been drawn in red in the central drawing [Fig. 13(b)]. Note that in Fig. 13(b), the original Fe atoms (existing in spinel) have been maintained together with the new (red) Fe atoms (existing in garnet). In this way, the transformation between both structures is clarified. It should be added that the diamond-like skeleton formed by the Si atoms in the spinel structure remains in the garnet. This is an additional indication that both compounds are strongly related.

Finally, it should be outlined that a garnet-like structure has been obtained in the MgSiO<sub>3</sub> catena-silicate under pressure.<sup>61</sup> This fact is not surprising if we look at its stoichiometry [Mg<sub>3</sub><sup>[8]</sup>(Mg, Si)<sup>[6]</sup>Si<sub>3</sub><sup>[4]</sup>O<sub>12</sub>]. Note that it is iso-electronic to both Fe<sub>3</sub>Fe<sub>2</sub>Si<sub>3</sub>O<sub>12</sub> and Nd<sub>3</sub>Al<sub>2</sub>Al<sub>3</sub>O<sub>12</sub> compounds. In connection with this, it could be speculated whether a garnet-like structure could exist for Al<sub>2</sub>O<sub>3</sub> (Al<sub>3</sub><sup>[8]</sup>Al<sub>2</sub><sup>[6]</sup>Al<sub>3</sub><sup>[4]</sup>O<sub>12</sub>).

## VI. CONCLUDING REMARKS

The high-pressure structural stability of Fe<sub>5</sub>Si<sub>3</sub> and Ni<sub>2</sub>Si have been studied by means of x-ray diffraction experiments as well as by *ab initio* calculations. In our experiments, we observed the absence of phase transitions in both Fe<sub>5</sub>Si<sub>3</sub> and δ-Ni<sub>2</sub>Si up to 75 GPa. We also found that the compression of Fe<sub>5</sub>Si<sub>3</sub> is rather isotropic, whereas the compression of Ni<sub>2</sub>Si is highly anisotropic. This anisotropic behavior seems to be correlated with the spatial orientation of the chemical bonds and the highly oriented valence-electron density of Ni<sub>2</sub>Si. The experimental results are supported by the *ab initio* total-energy calculations, which also predict the occurrence of a phase transition in Fe<sub>5</sub>Si<sub>3</sub> at 283 GPa from the hexagonal

*P6<sub>3</sub>/mcm* phase to a cubic phase belonging to space group *Ia3d* (the structure of the Fe<sub>5</sub>Si<sub>3</sub> cation subarray in the garnet Fe<sub>5</sub>Si<sub>3</sub>O<sub>12</sub>). On the other hand, the *ab initio* calculations predict that the orthorhombic *Pbnm* structure of δ-Ni<sub>2</sub>Si is the most stable structure at least up to 400 GPa. Finally, an EOS was determined for Fe<sub>5</sub>Si<sub>3</sub> (Ni<sub>2</sub>Si), giving the following parameters:  $V_0=187.154 \text{ \AA}^3$ ,  $B_0=215 \pm 14 \text{ GPa}$ , and  $B'_0=3.6 \pm 0.6$  ( $V_0=131.049 \text{ \AA}^3$ ,  $B_0=147 \pm 5 \text{ GPa}$ , and  $B'_0=4.5 \pm 0.5$ ) for the low-pressure phase and  $V_0=346.60 \text{ \AA}^3$ ,  $B_0=249.95 \text{ GPa}$ , and  $B'_0=3.77$  for the high-pressure phase of Fe<sub>5</sub>Si<sub>3</sub>. The prediction of the cubic phase (*Ia3d*) for Fe<sub>5</sub>Si<sub>3</sub>, under high pressure, is in agreement with the concept that relates oxidation and pressure.<sup>14,15</sup> The crystal chemistry of Fe<sub>5</sub>Si<sub>3</sub>, Fe<sub>2</sub>Si, and Ni<sub>2</sub>Si is also systematically discussed. It is shown that the Fe<sub>2</sub>Si structure, as well as the cation array in the olivine-like Fe<sub>2</sub>SiO<sub>4</sub>, can be seen as a continuous displacive transition from the Ni<sub>2</sub>Al-type structure. In the same way, a different structural relationship, with more physical meaning, can be established between the high-pressure phase of Fe<sub>2</sub>SiO<sub>4</sub> (spinel) and the garnet Fe<sub>5</sub>Si<sub>3</sub>O<sub>12</sub>.

## ACKNOWLEDGMENTS

This work was made possible through financial support of the MCYT of Spain under Grants Nos. MAT2004-05867-C03-01, MAT2004-05867-C03-02, MAT2004-05867-C03-03, MAT2007-65990-C03-01, and MAT2007-65990-C03-03. Three of the authors (D.E., P.R.-H., and A.M.) are also indebted to the MCYT of Spain for additionally supporting their own research with Grant No. CSD2007-00045. D.E. acknowledges the financial support from the MCYT of Spain through the "Ramón y Cajal" program. He also wants to thank the Alexander von Humboldt Foundation for its generous support. The U.S. Department of Energy, Office of Science, Office of Basic Energy Sciences supported the use of the Advanced Photon Source (APS) under Contract No. W-31-109-Eng-38. DOE-BES, DOE-NNSA, NSF, DOD-TACOM, and the W. M. Keck Foundation supported the use of the HPCAT facility. We would like to thank S. Sinogeikin, Y. Meng, and the rest of the staff at the HPCAT of the APS for their contribution to the success of the ADXRD experiments. We also thank O. Tschauer and R. Kumar from UNLV for sharing part of their beam time with us.

\*Author to whom correspondence should be addressed; FAX: (34) 96 354 3146; daniel.errandonea@uv.es

†Currently member of the MALTA Consolider Team.

<sup>1</sup>D. P. Dobson, L. Vocablo, and I. G. Wood, *Am. Mineral.* **87**, 784 (2002).

<sup>2</sup>J. F. Lin, A. J. Campbell, D. L. Heinz, and G. Y. Shen, *J. Geophys. Res.* **108**, 2045 (2003).

<sup>3</sup>D. Santamaria-Perez, J. Nuss, J. Haines, M. Jansen, and A. Vegas, *Solid State Sci.* **6**, 673 (2004).

<sup>4</sup>Y. Kuwayama and K. Hirose, *Am. Mineral.* **89**, 273 (2004).

<sup>5</sup>K. Takarabe, T. Ikai, Y. Mori, H. Udono, and I. Kikuma, *J. Appl.*

*Phys.* **96**, 4903 (2004).

<sup>6</sup>D. Santamaría-Pérez and R. Boehler, *Earth Planet. Sci. Lett.* **265**, 743 (2008).

<sup>7</sup>K. Tajima, Y. Endoh, J. E. Fischer, and G. Shirane, *Phys. Rev. B* **38**, 6954 (1988).

<sup>8</sup>D. Songlin, O. Tegus, E. Bruck, J. C. P. Klaase, F. R. De Boer, and K. H. J. Buschow, *J. Alloys Compd.* **334**, 249 (2002).

<sup>9</sup>F. Riedel and W. Schroter, *Phys. Rev. B* **62**, 7150 (2000).

<sup>10</sup>D. Leong, M. Harry, K. J. Reeson, and K. P. Homewood, *Nature (London)* **387**, 686 (1997).

<sup>11</sup>K. Takakura, T. Suemasu, Y. Ikura, and F. Hasegawa, *Jpn. J. Appl.*

- Phys., Part 2 **39**, L789 (2000).
- <sup>12</sup>H. Lange, *Phys. Status Solidi B* **101**, 3 (1997).
- <sup>13</sup>L. A. Martínez-Cruz, A. Ramos-Gallardo, and A. Vegas, *J. Solid State Chem.* **110**, 397 (1994).
- <sup>14</sup>A. Vegas, *Crystallogr. Rev.* **7**, 189 (2000).
- <sup>15</sup>A. Vegas and M. Jansen, *Acta Crystallogr., Sect. B: Struct. Sci.* **58**, 38 (2002).
- <sup>16</sup>A. Vegas, A. Grzechnik, K. Syasen, I. Loa, M. Hanfland, and M. Jansen, *Acta Crystallogr., Sect. B: Struct. Sci.* **57**, 151 (2001).
- <sup>17</sup>K. Toman, *Acta Crystallogr.* **5**, 319 (1952).
- <sup>18</sup>Y. R. Shen, R. S. Kumar, M. Pravica, and M. Nicol, *Rev. Sci. Instrum.* **75**, 4450 (2004).
- <sup>19</sup>D. Errandonea, Y. Meng, M. Somayazulu, and D. Häusermann, *Physica B* **355**, 116 (2005).
- <sup>20</sup>H. K. Mao, J. Xu, and P. M. Bell, *J. Geophys. Res.* **91**, 4673 (1986).
- <sup>21</sup>A. P. Hammersley, S. O. Svensson, M. Hanfland, A. N. Fitch, and D. Häusermann, *High Press. Res.* **14**, 235 (1996).
- <sup>22</sup>A. Boultif and D. Louer, *J. Appl. Crystallogr.* **24**, 987 (1991).
- <sup>23</sup>W. Kraus and G. Nolze, *J. Appl. Crystallogr.* **29**, 301 (1996).
- <sup>24</sup>G. Kresse and J. Furthmüller, *Comput. Mater. Sci.* **6**, 15 (1996); *Phys. Rev. B* **54**, 11169 (1996).
- <sup>25</sup>A. Mujica, A. Rubio, A. Muñoz, and R. J. Needs, *Rev. Mod. Phys.* **75**, 863 (2003).
- <sup>26</sup>J. P. Perdew, K. Burke, and M. Ernzerhof, *Phys. Rev. Lett.* **77**, 3865 (1996).
- <sup>27</sup>D. He and S. T. Duffy, *Phys. Rev. B* **73**, 134106 (2006).
- <sup>28</sup>D. Errandonea, R. Boehler, S. Japel, M. Mezouar, and L. R. Benedetti, *Phys. Rev. B* **73**, 092106 (2006).
- <sup>29</sup>O. Tschauer, J. McClure, and M. Nicol, *J. Synchrotron Radiat.* **12**, 626 (2005).
- <sup>30</sup>D. Errandonea, R. Boehler, B. Schwager, and M. Mezouar, *Phys. Rev. B* **75**, 014103 (2007).
- <sup>31</sup>D. Errandonea, J. Pellicer-Porres, F. J. Manjón, A. Segura, C. Ferrer-Roca, R. S. Kumar, O. Tschauer, P. Rodríguez-Hernandez, J. Lopez-Solano, S. Radescu, A. Mujica, A. Muñoz, and G. Aquilanti, *Phys. Rev. B* **72**, 174106 (2005).
- <sup>32</sup>I. G. Wood, W. I. F. David, S. Hull, and G. D. Price, *J. Appl. Crystallogr.* **29**, 215 (1996).
- <sup>33</sup>F. Birch, *J. Geophys. Res.* **83**, 1257 (1978).
- <sup>34</sup>L. Voadlo, G. D. Price, and I. G. Wood, *Acta Crystallogr., Sect. B: Struct. Sci.* **56**, 369 (2000).
- <sup>35</sup>K. Takarabe, R. Teranishi, J. Oinuma, and Y. Mori, *J. Phys.: Condens. Matter* **14**, 11007 (2002).
- <sup>36</sup>F. D. Murnaghan, *Proc. Natl. Acad. Sci. U.S.A.* **30**, 244 (1949).
- <sup>37</sup>D. P. Dobson, W. A. Crichton, P. Bouvier, L. Voadlo, and I. G. Wood, *Geophys. Res. Lett.* **30**, 1014 (2003).
- <sup>38</sup>N. Hirao, E. Ohtani, T. Kondo, and T. Kikegawa., *Phys. Chem. Miner.* **31**, 329 (2004).
- <sup>39</sup>E. G. Moroni, W. Wolf, J. Hafner, and R. Podloucky, *Phys. Rev. B* **59**, 12860 (1999).
- <sup>40</sup>S. Ono, T. Kikegawa, and Y. Ohishi, *Eur. J. Mineral.* **19**, 183 (2007).
- <sup>41</sup>R. Pöttgen, R.-D. Hoffmann, and D. Kußmann, *Z. Anorg. Allg. Chem.* **624**, 945 (1998).
- <sup>42</sup>M. Martínez-Ripoll and G. Brauer, *Acta Crystallogr., Sect. B: Struct. Crystallogr. Cryst. Chem.* **29**, 2717 (1973).
- <sup>43</sup>M. Chen, J. Shu, H. K. Mao, X. Xie, and R. J. Hemley, *Proc. Natl. Acad. Sci. U.S.A.* **100**, 14651 (2003).
- <sup>44</sup>H. Kudielka, *Z. Kristallogr.* **145**, 177 (1977).
- <sup>45</sup>A. Dewaele, P. Loubeyre, F. Occelli, M. Mezouar, P. I. Dorogokupets, and M. Torrent, *Phys. Rev. Lett.* **97**, 215504 (2006).
- <sup>46</sup>R. Boehler, *Nature (London)* **363**, 534 (1993); D. Errandonea, B. Schwager, R. Ditz, C. Gessmann, R. Boehler, and M. Ross, *Phys. Rev. B* **63**, 132104 (2001).
- <sup>47</sup>J. M. Herndon, *Proc. Natl. Acad. Sci. U.S.A.* **93**, 646 (1996).
- <sup>48</sup>A. Franciosi, J. H. Weaver, and F. A. Schmidt, *Phys. Rev. B* **26**, 546 (1982).
- <sup>49</sup>A. Vegas and M. Martínez-Ripoll, *Acta Crystallogr., Sect. B: Struct. Sci.* **48**, 747 (1992).
- <sup>50</sup>A. Vegas and V. García-Baonza, *Acta Crystallogr., Sect. B: Struct. Sci.* **63**, 339 (2007).
- <sup>51</sup>D. Errandonea, D. Martínez-García, A. Segura, A. Chevy, G. Tobias, E. Canadell, and P. Ordejón, *Phys. Rev. B* **73**, 235202 (2006).
- <sup>52</sup>H. Y. Chung, M. B. Weinberger, J. B. Levine, A. Kavner, J. M. Yang, S. H. Tolbert, and R. B. Kaner, *Science* **316**, 436 (2007).
- <sup>53</sup>F. Laves and H. J. Wallbaum, *Z. Kristallogr.* **101**, 78 (1939).
- <sup>54</sup>F. Laves and H. J. Wallbaum, *Z. Angew. Mineral.* **4**, 17 (1942).
- <sup>55</sup>R. W. Wyckoff, *Crystal Structures* (Wiley, New York, 1964).
- <sup>56</sup>S. I. Akimoto, H. Fujisawa, and T. Katsura, *J. Geophys. Res.* **70**, 1969 (1965).
- <sup>57</sup>G. Ottonello, M. Borketa, and P. F. Sciuto, *Am. Mineral.* **81**, 429 (1996).
- <sup>58</sup>A. F. Wells, *Structural Inorganic Chemistry* (Clarendon, Oxford, 1975).
- <sup>59</sup>M. O’Keeffe and B. G. Hyde, *Structure and Bonding* (Springer Verlag, Berlin, 1985), Vol. 61, pp. 77–144.
- <sup>60</sup>J. E. Jorgensen and S. E. Rasmussen, *Acta Crystallogr., Sect. B: Struct. Crystallogr. Cryst. Chem.* **38**, 346 (1982).
- <sup>61</sup>R. J. Angel, L. W. Finger, R. M. Hazen, M. Kanzaki, D. J. Weidner, R. C. Liebermann, and D. R. Veblen, *Am. Mineral.* **74**, 509 (1989).